



Active, long-lived upper-plate splay faulting revealed by thermochronology in the Alaska subduction zone



Suoya Fan ^{a,*}, Kristin D. Morell ^a, Donald M. Fisher ^b, Hugues Raimbourg ^c, Vincent Famin ^{d,e}, Kristijan Rajić ^f

^a Department of Earth Science, University of California, Santa Barbara, Santa Barbara, CA, USA

^b Department of Geosciences, Pennsylvania State University, University Park, PA, USA

^c Institut des Sciences de la Terre d'Orléans, Université d'Orléans/CNRS/BRGM UMR7327, 1A Rue de la Ferrière, Orléans 45100, France

^d Université Paris Cité, Institut de Physique du Globe de Paris, Paris, France

^e Laboratoire Géosciences Réunion, Université de La Réunion, Saint-Denis, France

^f Department of Earth Sciences, Durham University, Science Laboratories, South Road, Durham DH1 3LE, UK

ARTICLE INFO

Keywords:

Splay fault
Forearc tectonics
Alaska subduction zone
Thermochronology
Exhumation History

ABSTRACT

The lack of subaerial forearc geological records in active subduction zones has hindered our understanding of the roles of upper-plate structures and their interactions with plate interface processes in accommodating forearc deformation. Forearc splay faults, a type of upper-plate structure, are of particular interest due to their high efficiency in triggering tsunamis during great earthquakes. The coastal area of the Kodiak Islands, Alaska, USA exhibits stratigraphic and geomorphologic records of Miocene to Recent vertical tectonism and Quaternary thrust faults, suggesting potential splay-fault-involved deformation over geological timescales. To better understand the mechanisms of forearc long-term strain accumulation and the roles of splay faults, we investigate the spatial and temporal pattern of recent forearc exhumation in the Kodiak accretionary prism by conducting zircon and apatite (U-Th)/He (ZHe and AHe) thermochronologic analyses and thermal history modeling. These results are supplemented by field investigations, detrital zircon geochronology analyses and offshore active fault mapping. Most of the ZHe ages record cooling through the ZHe closure temperature in the late Eocene-early Oligocene, temporally and spatially consistent with the Eocene-early Oligocene broad antiformal exhumation previously documented by zircon and apatite fission track thermochronological ages. However, the AHe ages record cooling through the AHe closure temperature from early Miocene to Pliocene and exhibit an overall trenchward younging trend, with all the Pliocene ages (3–5 Ma) in the regions closest to the trench. Our thermal history modeling and field survey suggest that the trenchward coastal area of the Kodiak Islands experienced a change from early-middle Miocene basin subsidence to recent deformation and rapid uplift from 6–7 Ma to recent, while the rest of the island experienced an early-middle Miocene decrease in the prolonged exhumation from the Eocene-Oligocene. The newly revealed long-term exhumation pattern resembles the estimated uplift patterns based on elevated marine terraces and geodetic data. The early-middle Miocene change in exhumation pattern might be caused by a change in the dominant deformation mechanism affecting the Kodiak Islands, from broad underplating along the subduction interface mainly during the Eocene-Oligocene to hanging-wall uplift due to an active crustal splay thrust fault system since the late Miocene (the Kodiak Shelf Fault). We further discuss the dip-slip rate and geometry of the Kodiak Shelf Fault system and how inherited forearc upper-plate structures and lithology may affect forearc fluid distribution and facilitate the development and persistent deformation of the Kodiak Shelf Fault system.

1. Introduction

Investigating the long-term activity, geometry, lifespan, and

evolution of forearc upper-plate structures in subduction zones is critical to understanding the growth mechanisms of accretionary complexes, which involve complex and dynamic interactions between plate-

* Corresponding author.

E-mail addresses: fansy07@gmail.com, suoyafan@ucsb.edu (S. Fan).

interface and upper-plate processes. Many studies have aimed to better understand these interactions by correlating upper-plate structures, topography, and basins with subduction interface properties and earthquake patterns (e.g., Wells et al., 2003; Saillard et al., 2017; Dielforder et al., 2020; Jolivet et al., 2020; Michel-Wolf et al., 2022; Oryan et al., 2024). Deep-rooted crustal splay faulting, for example, can be a major thickening mechanism in the forearc, as indicated by out-of-sequence thrusts archived in exposed forearc accretionary complexes, such as the Kodiak accretionary complex in Alaska, USA (Rowe et al., 2009; Farris, 2010; Wilson, 2013). The active equivalents of these faults, forearc active splay faults, tend to be located near the rheological transition at the up-dip edge of the seismogenic zones (Wang and Hu, 2006; Kimura et al., 2007; Wang and Morgan, 2022). This observation and records of their direct involvement in tsunami-triggering processes during great earthquakes, further highlights the significance of understanding active splay faults in assessing seismic and tsunami hazards (e.g., Plafker, 1965; Cummins and Kaneda, 2000; Sibuet et al., 2007). However, the long-term history, including the initiation, lifespan, cessation, and reactivation of currently active splay faults, is rarely well studied.

Splay faults have been proposed to efficiently transfer deep displacement to the surface, fostering tsunami genesis (Moore et al., 2007; Wendt et al., 2009; van Zelst et al., 2022). Previous studies suggest that the coseismic rupture of a forearc splay fault in the Prince William Sound fostered the genesis of a large tsunami in the Alaska subduction zone during the 1964 M9.2 Great Alaska earthquake (Plafker, 1965; Suito and Freymueller, 2009; Suleimani and Freymueller, 2020) and its repeated ruptures have contributed to long-term permanent forearc uplift (Liberty et al., 2013; Haeussler et al., 2015; DePaolis et al., 2024). The involvement of splay fault rupture has also been suggested in other great tsunamigenic subduction zone earthquakes, such as the 1944 M8.1 Tonankai earthquake and the 1946 M8.3 Nankai earthquake in Japan (Cummins and Kaneda, 2000; Park et al., 2002), as well as the 2004 Mw9.2 Sumatra earthquake (Sibuet et al., 2007).

Splay faults located in the general region near the up-dip edge of the seismogenic zone have been well-documented, with examples such as Nankai (Park et al., 2002; Kimura et al., 2007; Moore et al., 2007; Strasser et al., 2009), Sumatra (Cook et al., 2014; Qin et al., 2024), and Hikurangi (Barker et al., 2018; Barnes et al., 2020). Similarly, offshore surveys in the Alaska subduction zone have primarily focused on the forearc frontal part straddling the up-dip limit of the seismogenic zone (e.g., Li et al., 2018; von Huene et al., 2021). However, the geometry and long-term evolution of active splay faults located in the forearc farther inboard are generally poorly understood, in large part because direct geological studies of these structures are often hindered by a lack of subaerial exposures and require deep seismic data.

The Kodiak Islands in the forearc of the highly-coupled Alaska subduction zone, located ~140 km from the trench, is an ideal area to probe the geometry and rates of splay faulting in the inner forearc. The trenchward coastal area of the Kodiak Islands is located approximately above the present down-dip edge of the seismogenic zone and exhibits stratigraphic and geomorphologic records of Miocene to Recent vertical tectonism and includes a series of Quaternary active faults (e.g., Clendenen et al., 1992; Carver et al., 2008; Elliott and Freymueller, 2020). These active faults are interpreted as a part of the Kodiak Shelf Fault Zone, a major offshore crustal splay fault zone that has been proposed to have ruptured during the 1964 Great Alaska earthquake and was the potential source of a local Kodiak Islands tsunami (Ramos et al., 2022). These co-located indicators of forearc deformation across a wide range of timescales suggest a potential causal relationship between the persistent activity of the Kodiak Shelf Fault Zone and long-term upper-plate vertical tectonism, as evidenced by uplifted and deformed Miocene shelf-basin strata. However, testing this hypothesis requires a better understanding of the Kodiak Shelf Fault Zone, including its kinematics, deep geometry, deformation rates, and slip history.

To better understand the rates, history, and spatial distribution of

forearc deformation across the Kodiak Shelf Fault Zone, its relation to deep accretionary complex structures and its connectivity with the subduction interface, we investigate the spatial-temporal exhumation patterns of the Kodiak Islands with a focus on the post-Oligocene history of the trenchward coastal area. We conduct new low-temperature zircon and apatite (U-Th)/He (ZHe and AHe) thermochronology analyses together with thermal history modeling and detrital zircon geochronologic analyses. The AHe ages reveal a previously unrecognized rapid exhumation pattern that we interpret to be primarily controlled by displacement along the Kodiak Shelf Fault Zone. The ZHe and AHe ages suggest a significant change in forearc dominant deformation style in the early-middle Miocene. The new deformation pattern after the style change indicates persistent deformation of the Kodiak Shelf Fault Zone from 6–7 Ma to present. We further infer a deep fault geometry and compare it with published forearc geophysical data to discuss how the inherited upper-plate structures and lithologic architecture may affect regional fluid distribution and facilitate the development and persistent deformation of the Kodiak Shelf Fault.

2. Geology

2.1. Tectonostratigraphy of the Kodiak Islands

The Kodiak Islands represent the subaerial part of the Kodiak accretionary complex, comprising a series of trench-parallel-striking rock packages that decrease in age and metamorphic grade trenchward (Moore et al., 1983) (Fig. 1). These rock packages were accreted episodically since the Jurassic through underplating or frontal accretion (Moore and Allwardt, 1980; Byrne and Fisher, 1987; Fisher and Byrne, 1987, 1992; Clendenen et al., 2003; Rajić et al., 2023). The northwestern edge of the Kodiak Islands comprises an island arc assemblage of late Triassic to early Jurassic ages and the Jurassic Raspberry Schist (Carden et al., 1977; Burns, 1985; Roeske et al., 1989). The Border Ranges Fault juxtaposes these rocks against the Uyak Complex, a tectonic mélange with rocks that contain fossils of mid-Permian to mid-early Cretaceous age (Connelly, 1978). The Uyak Complex is in tectonic contact with the Kodiak Formation southeast of it along the Uganik Thrust (Moore, 1978; Rowe et al., 2009).

The Kodiak Formation is a mostly structurally coherent, thick sequence of deep-water turbidites, including interbedded slates, siltstones, and sandstones, deposited in the Maastrichtian ~70 Ma ago (Byrne and Fisher, 1987; Sample and Reid, 2003). It occupies most of the Kodiak Islands and forms a regional anticlinorium (Sample and Moore, 1987; Fisher and Byrne, 1992; Rajić et al., 2023). The Kodiak Formation is separated from the Paleocene Ghost Rocks Formation by the Contact Fault (Fig. 1; Farris, 2010; Wilson, 2013). The Ghost Rocks Formation consists of a structurally coherent unit in the northwest and a tectonic mélange in the southeast (Byrne, 1984). The accretion of the Kodiak Formation and Ghost Rocks Formation occurred from the late Cretaceous to the early Paleogene (Byrne, 1984; Byrne and Fisher, 1987), and the youngest temporal limit is well bracketed by the ages of temporally close (about 58–62 Ma) but widely distributed intrusive rocks (Moore et al., 1983; Byrne and Fisher, 1987; Sample and Moore, 1987; Farris et al., 2006; Farris, 2010). These intrusive rocks are mostly andesite and granodiorite with some mafic rocks and are interpreted to be caused by west-to-east migrating ridge subduction and the interaction of MORB-type magmas with the metasedimentary rocks in the accretionary prism (Moore et al., 1983; Haeussler et al., 2003; Farris et al., 2006). The largest pluton is the Kodiak Batholith, the exposure of which trends sub-parallel with the long axis of the islands (Fig. 1).

The Eocene Sitkalidak Formation, in fault contact with the Ghost Rocks Formation, is a deep-sea fan sequence consisting of sandstone, siltstone, mudstone, and conglomerate and outcrops along the southeastern edge of the Kodiak Islands (Figs. 1 and 2), including the Ugak Island (Nilsen and Moore, 1979; Moore and Allwardt, 1980). It contains two structural units: a less deformed portion interpreted as a shortened

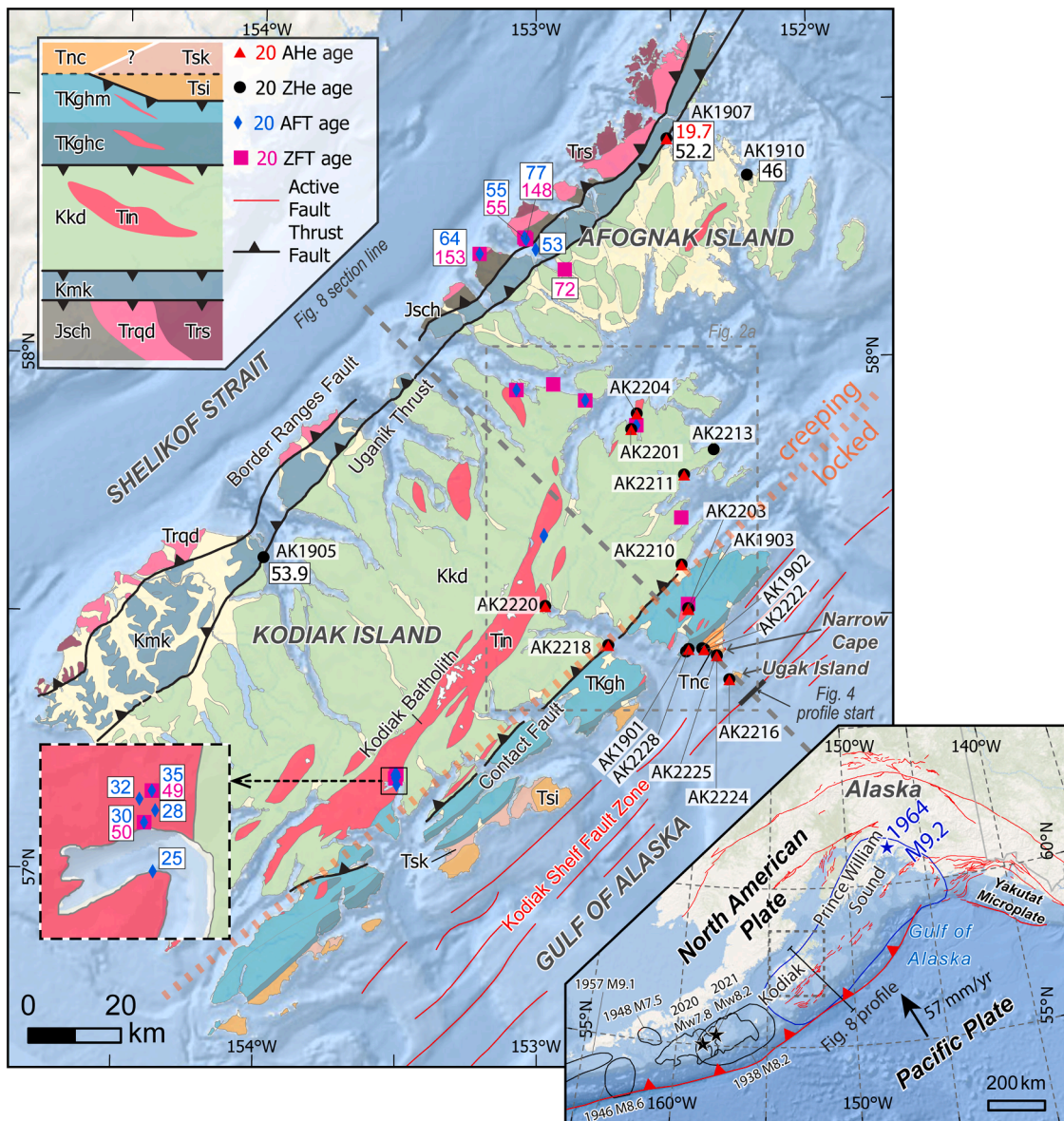


Fig. 1. Geological map of Kodiak Islands area (Wilson, 2013) with sample locations and a subset of the new thermochronology ages. Zircon and apatite (U-Th)/He (ZHe and AHe) ages are new data and their sample names are labeled. Zircon fission track (ZFT) and apatite fission track (AFT) ages are from Clendenen et al. (2003). Age numbers in the same box are from the same sample. Ages within the gray dashed rectangle are shown in Fig. 2. The locked-creeping boundary is based on Elliott and Freymueller (2020). The inset map in the lower-left corner shows the details of a sample cluster. The regional map in the lower-right shows plate boundaries, rupture areas of forearc large earthquakes (circles; Davies et al., 1981; Liu et al., 2022), Quaternary faults (red lines; from U.S. Geological Survey), the main map extent (gray dashed box) and the profile line. Map units: Tnc – Narrow Cape Formation, Tsk – Sitkinak Formation, Tsi – Sitkalidak Formation, TKghm – Ghost Rocks Formation mélange unit, TKghc – Ghost Rocks Formation coherent unit, Kkd – Kodiak Formation, Tin – Paleogene intrusive rocks, Kmk – Uyak Complex, Jsch – Raspberry schist, Trqd – Triassic Afognak pluton, Trs – Triassic sedimentary unit.

slope basin or slope apron deposit and a strongly deformed portion featured by landward verging folds and thrusts interpreted as trench-filling sediment offscraped from the lower plate (Moore and Allwardt, 1980).

Oligocene-Pleistocene slope basin fill overlies the Ghost Rocks and Sitkalidak Formations above an angular unconformity, and it contains several units of different ages along the southeastern margin of the Kodiak Islands (Moore and Allwardt, 1980; Clendenen et al., 1992; Marincovich and Moriya, 1992). In the Narrow Cape area, the sequence above the unconformity is the slightly younger middle Miocene Narrow Cape Formation comprising shallow marine sandstone and sandy siltstone, with interbedded conglomerate beds (Moore et al., 1983). The age of the Narrow Cape Formation is interpreted to be 15–16 Ma based on well-dated faunas (Marincovich and Moriya, 1992). The

Oligocene-Miocene unconformity has been interpreted to be correlated seaward to an unconformity visible in seismic reflection profiles in the offshore region (Fisher and Holmes, 1980; Moore and Allwardt, 1980; Clendenen et al., 1992). The offshore part of the post-unconformity basin has continuously received sediments up until the present day. The current trenchward boundary of the shelf-basin is approximately located at the present-day shelf break, about 60–80 km trenchward from the landward boundary exposed on the Kodiak Islands. The subaerial basin recorded by the Narrow Cape Formation in the Kodiak coastal area may represent the deformed and uplifted part of this same basin.

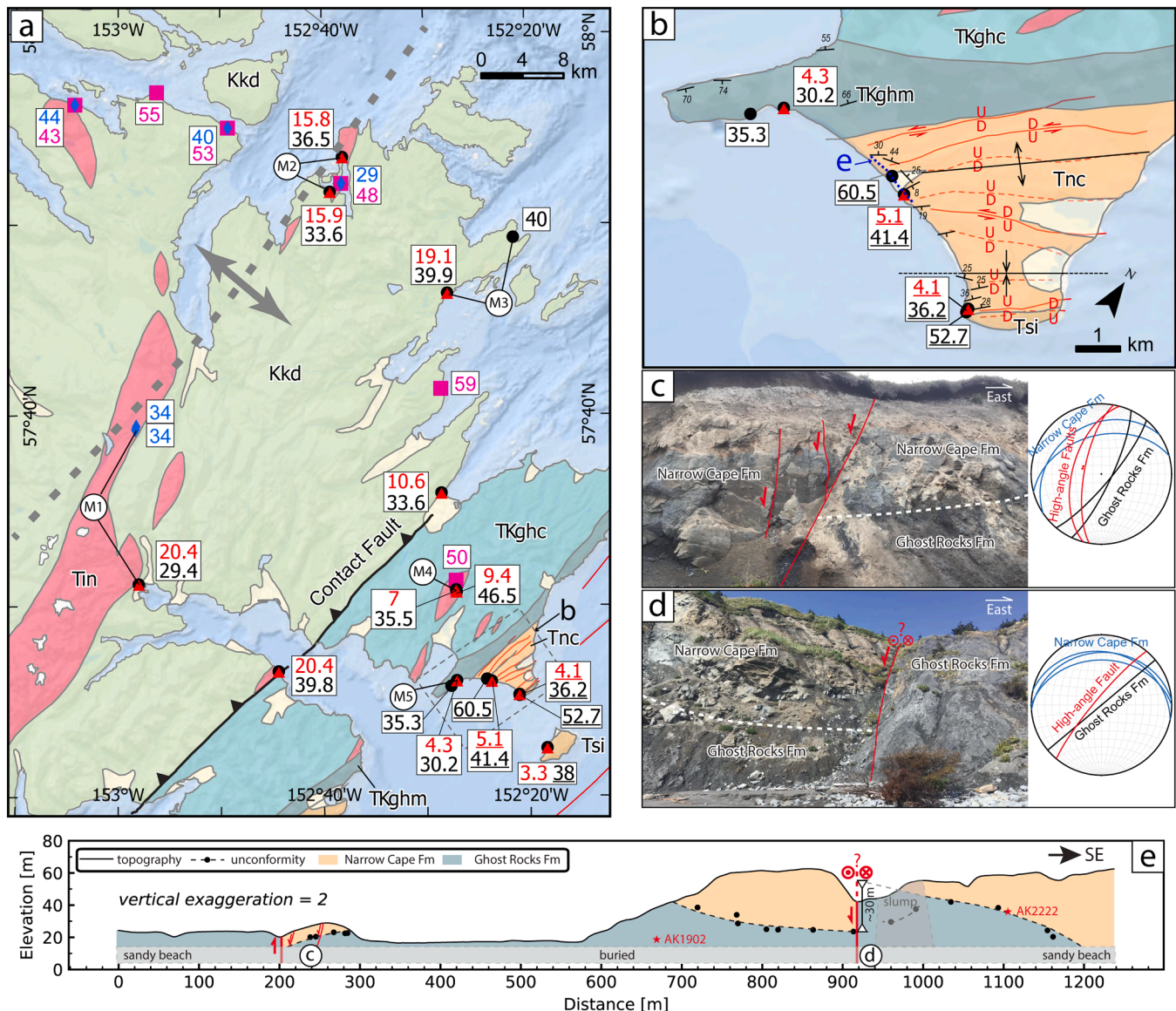


Fig. 2. (a) Geological map of the main sample area with thermochronological ages. Underlined numbers indicate the youngest grain age of the sample. M1-M5 are locations of thermal history models in Fig. 6. (b) Detailed map of the Narrow Cape Fm area. Active faults were mapped by Carver et al. (2008). Other map symbols are the same as Fig. 1. (c-d) Field photos show high-angle faults that cut the Narrow Cape Formation and unconformity and stereonet plots of faults, kinematic indicators and bedding at the two localities. (e) A profile along the coastal cliff shows cliff topography, unconformity elevation (black dots are field measurements), sample locations (red stars), and high-angle faults. The topographic profile is extracted along the dotted blue line in (b) and projected to a straight line subparallel to the coast.

2.2. Cretaceous-Cenozoic deformation, exhumation and active tectonics

2.2.1. Cretaceous to Miocene

Two main episodes of deformation and exhumation before the Miocene have been recognized in the Kodiak Islands. The first episode is represented by the accretion of the Kodiak and Ghost Rocks Formations, mainly through underplating along the subduction interface from the late Cretaceous to the early Paleocene. Evidence for underplating includes the regional anticlinorium, duplex structures in both mesoscopic and map scales, and across-strike changes in deformation style, magnitude and structural orientation (Sample and Fisher, 1986; Fisher and Byrne, 1987; Sample and Moore, 1987, 1992; Rajić et al., 2023). The peak temperature and amount of exhumation experienced by the Kodiak and Ghost Rocks Formations also mimic the antiformal pattern with the highest magnitude in the core of the anticlinorium (Clendenen et al., 2003; Rajić et al., 2023). The second episode of exhumation and thickening occurred from Eocene to Oligocene and has been interpreted as a

result of trenchward-propagating underplating. Evidence for this process is based on a thermochronologic study involving zircon and apatite fission track (ZFT and AFT) dating that shows cooling ages become younger trenchward from the northwestern limit of the Kodiak Formation to the Kodiak Batholith (Clendenen et al., 2003). Moreover, an offshore seismic reflection profile northeast of the Kodiak Islands exhibits arched reflectors that coincide with a thick low-velocity zone below the Mesozoic and Paleocene accretionary prism, consistent with underplating (Byrne, 1986; Moore et al., 1991; Ye et al., 1997).

2.2.2. Miocene to Quaternary

Paleoseismic, geodetic, stratigraphic, and field data together provide several lines of evidence for Quaternary-active deformation within the Narrow Cape and surrounding area of the Kodiak Islands. Geomorphology and paleoseismology surveys in the Narrow Cape area have identified several near-vertical faults that have been reported to accommodate both vertical and strike-slip Quaternary displacement

(Carver et al., 2008). Carver et al. (2008) documented fault activity spanning the latest Pleistocene and Holocene and suggested the faults offset a marine terrace by up to 20 m and offset channels left-laterally by up to 30–35 m. Carver et al. (2008) interpreted the major faults as part of the Kodiak Shelf Fault Zone, a ~200-km-long margin-parallel active splay fault system (Fig. 1). In the field, we observed these faults cross-cutting the sub-horizontal angular unconformity separating the Ghost Rocks and Narrow Cape Formations by as much as ~30 m in the modern sea cliff (Fig. 2). The angular unconformity and the Narrow Cape Formation above it have been gently folded into an anticline and syncline; these folds are likely related to these active structures. Carver et al. (2008) recognized a group of coastal surfaces, characterized by a locally uniform elevation, planar sub-horizontal abrasion surfaces, with a sharp back-edge that parallels the shoreline. They interpreted them as raised wave-cut marine terraces formed during Marine Isotope Stage (MIS) 5e (120–130 ka). The elevation of these marine terraces across the Kodiak Islands also increases abruptly in the Narrow Cape area, suggesting a 3–5 times higher Quaternary uplift rate of the Narrow Cape area than areas arcward (Carver et al., 2008), although the source of this reported uplift is not described in previous literature. Campaign GNSS data collected over an 8-year period also exhibit the highest across-strike velocity spatial gradient in this region, suggesting left-lateral transpressional strain, in the Narrow Cape area (Sauber et al., 2006; Carver et al., 2008). The area also lies roughly above the locked-creeping transition zone along the subduction interface (Elliott and Freymueller, 2020).

In the trenchward region offshore within 15 km of the Narrow Cape

area of the Kodiak Islands, the Kodiak Shelf Fault Zone has been recognized and mapped based on seismic reflection images and bathymetry data (Ramos et al., 2022). The fault system contains multiple strands offshore, among which the most recognizable is the Ugak Thrust, located ~5 km seaward of Ugak Island (Figs. 1 and 3). Based on seismic reflection profiles, these faults have been reported to be landward dipping at 65–80° close to the seafloor and may merge at depth (Ramos et al., 2022). The Ugak Fault offsets the seafloor, forming a prominent bathymetric scarp, as much as 30 m high, and extends at least 80 km in length. Other high-angle faults have been previously identified cutting the slope basin strata but their recent activity remains unclear (Fisher and Holmes, 1980). Northeast of the Kodiak Islands, in the Prince William Sound segment, a similar splay fault system in the equivalent structural location in the forearc has been recognized and thought to have ruptured during the 1964 M9.2 earthquake, but there is no direct evidence connecting it to the Kodiak Shelf Fault Zone (Liberty et al., 2013; Haeussler et al., 2015, 2019; DePaolis et al., 2024). Although these previous studies provide evidence for Quaternary activity, mainly in the form of faulting and folding in the Narrow Cape region, how long these structures have been active, their exhumation histories, throw rates, and potential relationship to the underplating and duplexing structures remain poorly understood.

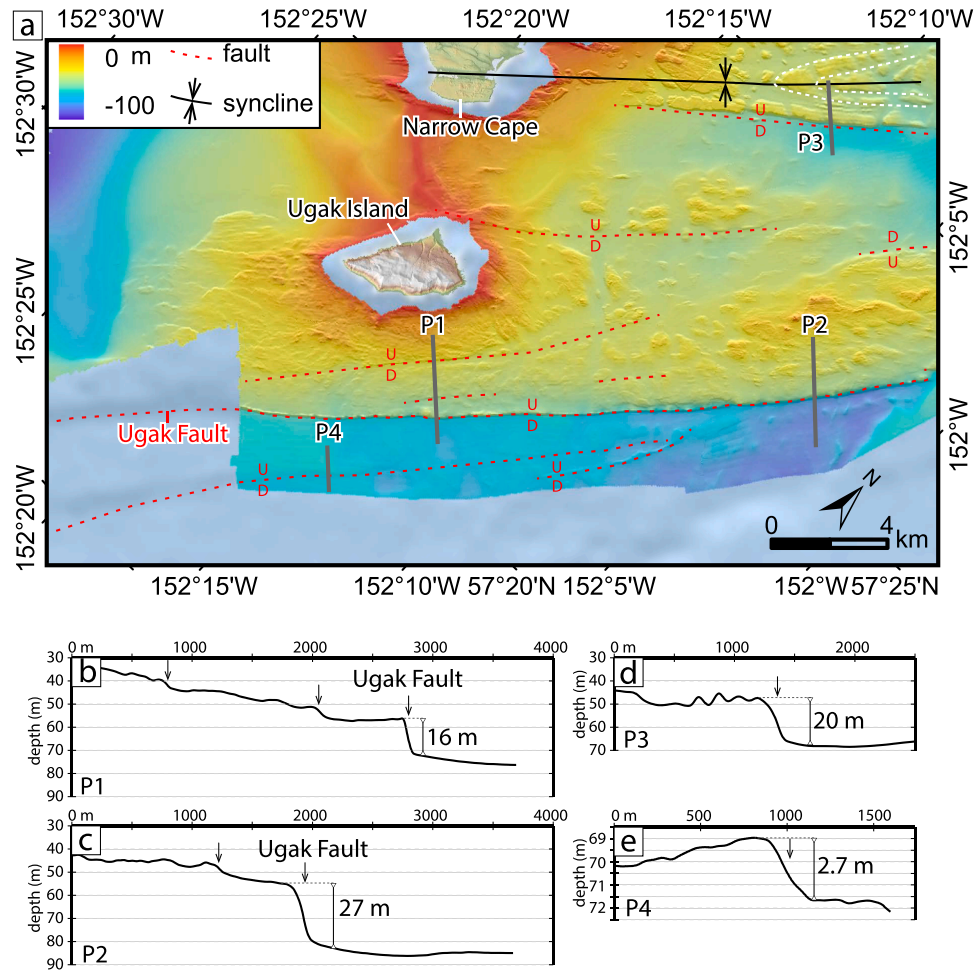


Fig. 3. Bathymetry map (a) and topographic profiles (b–e) show the active Kodiak Shelf Fault Zone. U – up, D – down. Black arrows in b and c indicate topographic scarps. Note that profile P4 has a different scale from profile P1–P3.

3. Thermochronology and geochronology

3.1. Methods and samples

To investigate post-Oligocene to Quaternary exhumation mechanisms of the Kodiak Islands, we conducted ZHe and AHe thermochronologic analyses on samples collected along a trench-perpendicular transect (Fig. 1; Table 1). The closure temperatures of the zircon and apatite thermochronometers are affected by various factors, such as the chemical composition of the minerals, concentration of radiation damage, grain size and cooling rate (Reiners et al., 2004; Reiners, 2005) but typically range from ~ 170 – 190 °C (Reiners et al., 2004) and ~ 45 – 70 °C (Flowers et al., 2009). We obtained 19 ZHe and 13 AHe ages from 19 samples across the Kodiak Islands (Figs. 1 and 2; Tables 1 and S1), from the Uyak Complex along the landward coast to Ugak Island in the trenchward coastal area. We increased sampling density in the southeastern half of the transect. Our sampling strategy was to first attempt to sample 60-Ma plutonic rocks, because we found that these samples contained the largest suitable apatite and zircon grains for dating. When these rock types were not available along the transect, we also sampled low-grade metamorphic rocks of the Kodiak and Ghost Rocks Formation, sandstones from the Sitkalidak and Narrow Cape Formations, and two samples from the Uyak Complex. We collected samples with the largest visible grain size. The supplementary information contains the details of our sample processing and dating analysis.

In addition to thermochronology, we also conducted detrital zircon (U-Pb) geochronologic analyses on two Narrow Cape samples and one Sitkalidak Formation sample to understand their provenance and depositional ages. The Sitkalidak Formation sample was collected from Ugak Island, and the Narrow Cape Formation samples are collected directly above its unconformable contact with the Ghost Rocks Formation (Fig. 2).

3.2. Results

The AHe ages range from 20 to 3 Ma, showing an overall decrease in age trenchward for the 30-km-long area northeast of Ugak Island (Figs. 2 and 4). The ages in the region from the Uyak Complex to the Contact Fault are generally spatially invariant at 15–20 Ma for 70 km across strike. Neither the Uganik thrust nor the Contact Fault show variations in cooling ages across them, suggesting no significant faulting-related exhumation along these onshore major faults since the Miocene. The AHe cooling ages from the plutonic rock that intruded into the Ghost

Rocks Formation and further trenchward are all younger than 10 Ma, and the four samples closest to the offshore Kodiak Shelf Fault Zone, within 20 km from the Ugak Fault, yielded Pliocene cooling ages (3–5 Ma). Two of the Pliocene cooling ages are derived from the youngest grain age in each sample from the Narrow Cape Formation. These samples exhibit a wide dispersion of AHe grain ages, including ages younger than the middle Miocene depositional age, indicating partial thermal resetting of the samples during burial heating. Because their youngest grain ages (4.1 ± 0.2 Ma and 5.1 ± 0.2 Ma) are close to the mean aliquot ages of the fully thermally-reset Sitkalidak Formation (3.3 ± 0.3 Ma) and Ghost Rocks Formation (4.3 ± 0.6 Ma), we interpret these youngest grains as being fully or nearly fully reset before recent cooling through the AHe partial retention temperature zone.

The ZHe age range overall overlaps with the published AFT ages and is younger than the ZFT ages in the area of data coverage (>38 km on the age-distance profile in Fig. 4). These ZHe ages exhibit an overall decrease in cooling ages from 52–54 Ma for samples of the early Cretaceous Uyak Complex on the landward side of the Kodiak Islands to 30–34 Ma of the Kodiak Batholith (58–59 Ma U-Pb zircon ages; Farris, 2010). This age spatial variation pattern resembles the AFT age spatial pattern reported by Clendenen et al. (2003).

The ZHe, AFT and ZFT samples all progressively decrease in age from the arcward coast to the Kodiak Batholith. In contrast, the ZHe ages further trenchward, located about 0–38 km on the age profile (Fig. 4), are invariant in age along strike, with samples in this region close to or slightly older than the ZHe ages of the Kodiak Batholith. Among them, the five samples closest to the Ugak Thrust are not thermally reset after deposition: four samples from the Narrow Cape Formation and Sitkalidak Formation yield dispersed grain ages older than their depositional ages. One sample from the Ghost Rocks formation in the Narrow Cape area close to the unconformity generated grain ages of 60–67 Ma, much older than the ZHe ages of two other Ghost Rocks Formation samples (30 and 35 Ma) near a basalt intrusion and the ages of the pluton rock intruded into the Ghost Rocks Formation.

The U-Pb detrital zircon ages of the Sitkalidak Formation and the Narrow Cape Formation samples mostly range from 50 Ma to 220 Ma (Table S2). The probability density curve peaks at around 60 Ma, a broad high age spectrum ranging from 60 to 110 Ma, and a low broad age spectrum of 130–220 Ma, mainly straddling the Jurassic (Fig. 5). The youngest ages are much older than the depositional ages of the two formations (Eocene-early Oligocene and mid-late Miocene, respectively); therefore, they do not provide meaningful estimation of maximum depositional ages. The 60 Ma peak coincides with the narrow

Table 1
Sample information and interpreted thermochronologic ages.

Sample ID	Latitude	Longitude	Elevation (m)	Rock Unit	ZHe (Ma)*	AHe (Ma)*
AK2201	57.862190	−152.653643	7.7	Paleogene Pluton	33.6 ± 1.9	15.9 ± 0.8
AK2203	57.514318	−152.451663	86.1	Paleogene Pluton	35.5 ± 3.8	7.0 ± 0.8
AK2204	57.892507	−152.633262	0.0	Paleogene Pluton	36.5 ± 1.0	15.8 ± 1.8
AK2210	57.599029	−152.474215	28.4	Kodiak Fm.	33.6 ± 3.8	10.6 ± 1.3
AK2211	57.773516	−152.462683	53.6	Kodiak Fm.	39.9 ± 1.9	19.1 ± 1.2
AK2213	57.821888	−152.354314	6.1	Kodiak Fm.	40.0 ± 2.2	—
AK2216	57.375702	−152.306023	0.8	Sitkalidak Fm.	38.0 ± 1.2	3.3 ± 0.3
AK2218	57.443505	−152.73995	9.8	Paleogene Pluton	39.8 ± 2.8	20.4 ± 2.0
AK2220	57.519658	−152.966643	19.1	Paleogene Pluton	29.4 ± 1.5	20.4 ± 1.1
AK2222	57.434397	−152.395072	12.1	Narrow Cape Fm.	41.4 ± 1.2	5.1 ± 0.2
AK2224	57.421713	−152.350214	8.7	Narrow Cape Fm.	52.7 ± 1.2	—
AK2225	57.422501	−152.350341	21.6	Narrow Cape Fm.	36.2 ± 0.8	4.1 ± 0.2
AK2228	57.435045	−152.451337	23.2	Ghost Rock Fm.	30.2 ± 0.7	4.3 ± 0.6
AK1901	57.430151	−152.460473	23.2	Ghost Rock Fm.	35.3 ± 2.2	—
AK1902	57.436105	−152.402721	12.1	Ghost Rock Fm.	60.5 ± 2.4	—
AK1903	57.512531	−152.450838	86.1	Paleogene Pluton	46.5 ± 2.4	9.4 ± 0.9
AK1905	57.610437	−153.984116	0.0	Kodiak Fm.	53.9 ± 3.3	—
AK1907	58.425533	−152.517855	0.0	Uyak Complex	52.2 ± 2.0	19.7 ± 4.4
AK1910	58.353702	−152.222284	0.0	Kodiak Fm.	46.0 ± 0.7	—

* Italic font indicates the youngest grain ages and the 2σ analytical uncertainties of the samples show highly dispersed grain ages. Other ages are mean grain ages and their standard errors.

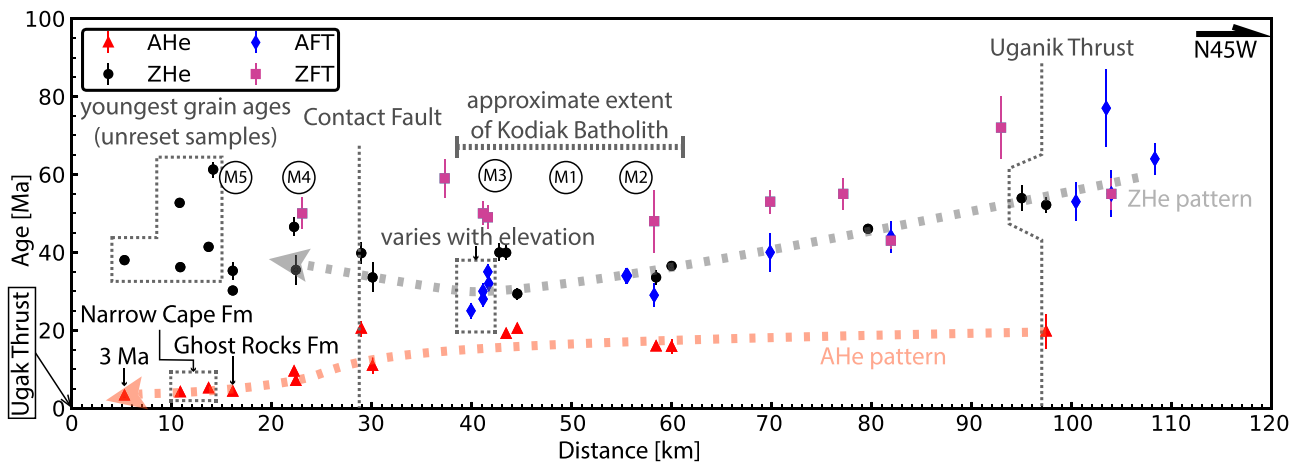


Fig. 4. Thermochronology age profile. The profile starts at the offshore Ugak Fault (Distance = 186 km on Fig. 8 profile) and is made along the thick gray dash line in Fig. 1. The zircon and apatite (U-Th)/He (ZHe and AHe) ages are from this study. The zircon and apatite fission track (ZFT and AFT) ages are from Clendenen et al. (2003). The five ZHe samples closest to the Ugak Fault in the dashed gray polygon are not thermally reset for ZHe system after deposition (refer to text for details) and for each of these samples, only the youngest grain age is plotted. AFT ages at about 40 km are from the sample cluster shown in the inset map in Fig. 1. Their ages vary with elevation (see Supplementary Information). Labels M1-M5 represent the approximate locations of the thermal history models along the profile.

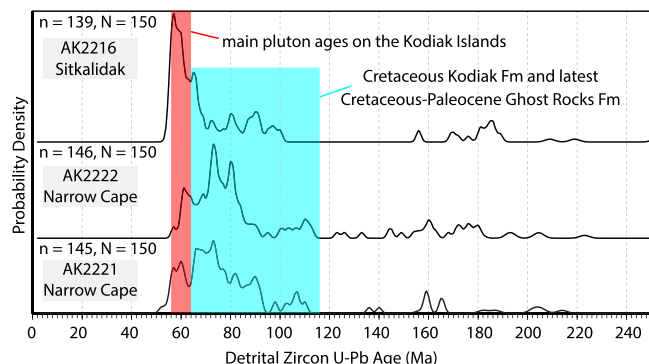


Fig. 5. Probability density plots of detrital zircon U-Pb ages of the Narrow Cape Formation and Sitkalidak Formation. The plots only show the ages younger than 250 Ma, which are the main component of the data. For each sample, N and n are the number of zircons analyzed and the number of ages younger than 250 Ma, respectively. The complete dataset is reported in Table S2.

age range of the widely distributed igneous rocks, represented by the Kodiak Batholith. The broad high spectrum of the Cretaceous ages and the low, broad spectrum of the Jurassic ages can be correlated with the widely distributed Cretaceous Kodiak Formation and the Jurassic accretionary complex and plutons on the northwestern edge of the Kodiak Islands. Therefore, the data support the idea that the Sitkalidak and Narrow Cape Formations might be mainly sourced from the Kodiak Islands and record the broad exhumation of the island during their deposition from the Eocene to Miocene.

4. Thermal history modeling

The variations in thermochronology ages along the transect and the source-to-sink history associated with the deposition of the Sitkalidak and Narrow Cape Formations, all indicate spatial variations in erosion and deposition of the Kodiak Islands. To further investigate the magnitude and timing of exhumation across the transect, we conducted one-dimensional thermal history modeling using the HeFTy (Ketcham, 2005) program with our new data. The temperature-time constraints used in the HeFTy modeling were based on geological context, published nearby thermochronologic data from Clendenen et al. (2003) and peak temperature estimations from Rajić et al. (2023) (Figs. 2 and 6). Considering the higher data density and higher cooling age contrast in

the southeastern half of the Kodiak Islands, we selected five modeling localities between the Kodiak Batholith, where the minimum ZHe, AFT, and ZFT ages have been reported, and the Ghost Rocks Formation in the trenchward coastal area of the islands, where the youngest AHe ages are located (Fig. 4). Models 1 and 2 are the farthest and of similar distance from the trench, but they are 43 km apart along strike. Models 2 to 5 are progressively closer to the trench. For detailed descriptions, modeled age data, thermal history constraints, and the geological context considered in each model, refer to the text and Table S3 in the Supplementary Information.

The thermochronologic data and modeling results show that the previously recognized Eocene-Oligocene broad cooling lasted until the early Miocene (15–20 Ma). After that, the trenchward coastal area and the central part of the Kodiak Islands exhibit distinct thermal histories. During approximately the middle-late Miocene, the central part of the Kodiak Islands (Models 1–3) changed to a slow cooling path, while the trenchward coastal area (Models 4 and 5), mainly the area of Ghost Rocks Formation and Narrow Cape Formation, experienced a transition from cooling to reheating, which was associated with the change from erosion to deposition along the angular unconformity beneath the forearc basin sediments of the Narrow Cape Formation. Some possible temperature-time paths with a good fit suggest a possible short period of accelerated cooling during the transitional phase (around 15–20 Ma) preceding the slow cooling phase in the central part of Kodiak Islands; but this possible acceleration in cooling is not required in all temperature-time paths with a good fit. Since the latest Miocene, the trenchward coastal area of the islands has been experiencing rapid cooling.

5. Discussion

5.1. Exhumation history

Our new ZHe ages and published ZFT and AFT ages are consistent with the previous interpretation that the Kodiak Islands experienced broad antiformal thickening and exhumation from the Eocene to Oligocene that straddles the Kodiak Islands (Clendenen et al., 2003). Structural and geophysical observations suggest the underplating process might have caused this regional thickening and exhumation pattern with a hinge line located in the central part of the Kodiak Islands (e.g., Byrne, 1986; Fisher and Byrne, 1992; Ye et al., 1997). Our ZHe ages and fission track ages of previous researchers (Clendenen et al., 2003) agree with this pattern as evidenced by their across-strike long-wavelength

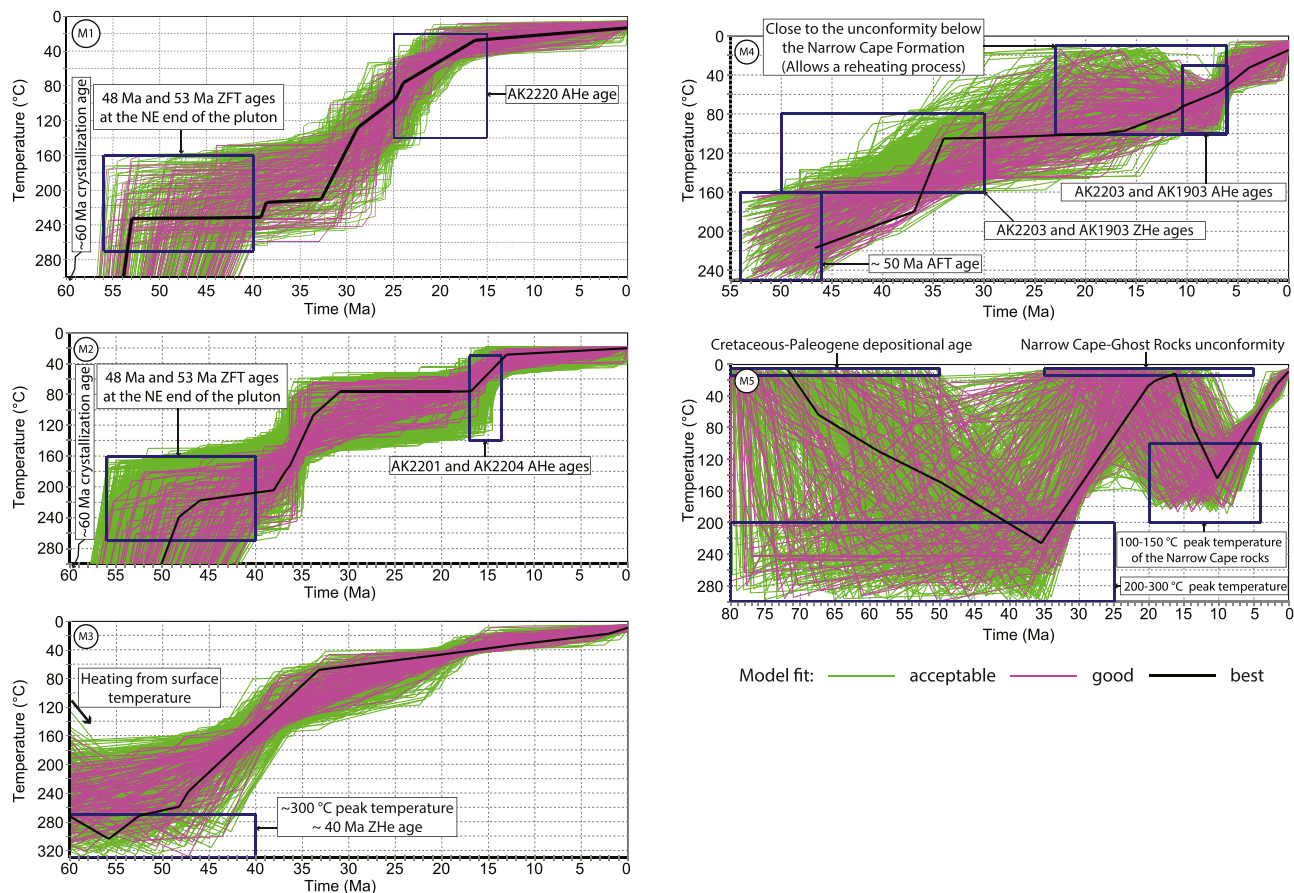


Fig. 6. Thermal history modeling results using HeFTy version 1.9.3 (Ketcham, 2005). The modeled locations are shown in Figs. 2 and 4. Constraints in each model are based on geological context, geochronology and thermochronology ages (Supplementary Information), and peak temperature estimations reported by (Rajić et al., 2023).

gradual change with the youngest ages in the Kodiak Batholith area in the central part of the Kodiak Islands (Fig. 4). This interpretation is further supported by Raman spectroscopy of carbonaceous materials that reveals a similar pattern of peak temperature: relatively high-temperature records broadly distributed in the central part of the Kodiak Islands with decreased temperature records in both trenchward and landward coastal areas (Rajić et al., 2023).

Our new AHe ages reveal a previously unrecognized cooling age pattern along the transect (Fig. 4). In the northwest, the AHe ages are relatively invariant, ranging from 15 to 20 Ma for ~60 km across strike from the Uyak Complex to the Kodiak Batholith. Moving trenchward, in the area occupied by the Ghost Rocks mélange and Narrow Cape Formations, the ages decrease to 4–5 Ma. Finally, at Ugak Island, ~5 km from the Ugak Fault, the AHe ages further decrease to 3 Ma. This AHe age pattern suggests that the previously recognized Eocene-Oligocene broad exhumation might have extended into the early Miocene in the central part of the Kodiak Islands, but the late Miocene-Pliocene exhumation may have been affected by a different deformation mechanism than the antiformal deformation that was occurring during the Eocene to Oligocene.

The difference in uplift and subsidence history between the trenchward coastal area of the Kodiak Islands and the area farther arcward is investigated with our one-dimensional thermal history models that incorporate constraints from geological observations (Fig. 6). In the area landward of the Contact Fault, represented by Models 1–3, the prolonged cooling in the Paleogene lasts through the Miocene. However, the cooling rate decreased after the early-middle Miocene (20–15 Ma) and has since maintained a slow cooling rate. In the meantime, the trenchward coastal area of the Kodiak Islands, the area represented by

Models 4 and 5, experienced a more complicated thermal history involving two cooling phases interrupted by a reheating process.

The first cooling episode of the trenchward coastal area of the Kodiak Islands might be caused by exhumation associated with the prolonged Oligocene to Miocene broad antiformal folding event, which may be related to underplating (Fig. 4). The unconformity between the Ghost Rocks and the Narrow Cape Formations, indicating uplift and erosion prior to the middle Miocene, may have formed during this period. The reheating process in Models 4 and 5 corresponds to the deposition of the Narrow Cape Formation, a subsidence and burial event, and temporally overlaps with the transition from fast to slow cooling in Models 1–3 (Fig. 6). These models suggest that the shelf subsidence in the Narrow Cape area indicated by the Narrow Cape basin formation is synchronous with a decrease, if not cessation, of the underplating process northwest of the basin below the Kodiak Islands. Previous stratigraphic and lithologic data of the shelf basin (Clendenen et al., 1992), our new detrital zircon U-Pb age spectrum, and the overlap between the range of the detrital ZHe ages of the Narrow Cape Formation and the cooling age range landward of the shelf basin, all suggest that the Kodiak Islands is the main source of sediment in the shelf basin along the Kodiak Islands coast in this period.

The second rapid cooling episode after the mid-late Miocene deposition and reheating along the trenchward coast of the Kodiak Islands (Models 4 and 5) is missing in the area represented by Models 1–3 (Fig. 6). Our thermal modeling results suggest that the initiation of this exhumation episode is no later than ~6 Ma (Fig. 6). The youngest basin fill along the Kodiak Islands coast, the late Pliocene-Pleistocene Tugidak Formation, locally overlies the along-strike equivalent of the Narrow Cape Formation on the Trinity Island about 150 km southwest of our

study area (Clendenen et al., 1992), suggesting that the initiation time of the latest rapid coast uplift should not be much older than the late Pliocene. The latest Miocene Albatross sedimentary sequence, the shelf basin record on the Trinity Islands, records a transition from a shallow-marine depositional environment to a terrestrial environment, suggesting an uplift process (Clendenen et al., 1992). These observations bracket the initiation time of the rapid uplift and exhumation at about 6–7 Ma.

5.2. Miocene-Quaternary exhumation pattern and the Kodiak Shelf Fault Zone

Assuming a thermal gradient of about 30 °C/km (Moore and Allwardt, 1980) and a peak temperature of 120 °C (Rajić et al., 2023) results in an exhumation rate of ~0.6–0.7 mm/yr and a total exhumation of about 4 km for the Miocene-Quaternary episode. This estimated exhumation rate is close to the inferred uplift rate of about 0.75 mm/yr based on the elevation of the uplifted coastal surface, assuming the surface formed during 130–120 ka (Carver et al., 2008).

To better evaluate the spatial variations in the new Miocene-Recent exhumation pattern revealed by the AHe ages, we calculated the exhumation rate for each AHe sample assuming steady, vertical rock uplift and unchanging topography (van der Beek and Schildgen, 2023). The results represent the averaged exhumation rate since the samples cooled through their closure temperatures. In three calculations, we assumed three initial geothermal gradients at 25 °C/km, 30 °C/km, and 35 °C/km, respectively. The result shows that the exhumation rate increases rapidly trenchward from about 0.1 mm/yr in the Kodiak Batholith area to about 0.5–0.7 mm/yr near Ugak Island (Fig. 7). The highest exhumation rates are located in the hanging wall of the Ugak Fault.

We also evaluate Quaternary uplift rates across the Kodiak Islands from the elevations of previously reported marine terraces, assuming they formed during MIS 5e, at about 125 ka following Carver et al. (2008). Although the terrace is not directly dated, Carver et al. (2008) speculate that the terrace must date to ~130–120 ka because paleosea level during MIS 5e represents the last time that paleosea level was higher than current sea level, and therefore is the last time that sea level occupied the position of the modern coastline. Although the marine terrace heights are likely affected by isostatic rebound following regional late Pleistocene deglaciation (Carver et al., 2008), and the assumed terrace uplift rates overall are higher than the calculated exhumation rates based on the AHe ages by about 0.15–0.2 mm/yr, they share a similar spatial pattern regardless of their age (Fig. 7). This pattern is also similar to the pattern revealed by current geodetic data, which shows the largest spatial gradient in the trenchward coastal area of the Kodiak Islands (Carver et al., 2008). The similarity of deformation patterns over decadal time spans represented by geodetics, millennial time scale recorded by marine terraces, and Myr time scale recorded by thermochronology suggests that the present deformation mechanism has controlled a persistent uplift pattern over a range of time scales.

Our ZHe ages and thermal modeling results, along with previous studies on rock cooling history, structures, peak temperatures, and seismic reflection profiles suggest that underplating along the plate interface could be the main mechanism of forearc wedge thickening in the Eocene-Oligocene (Byrne, 1986; Sample and Fisher, 1986; Moore et al., 1991; Fisher and Byrne, 1992; Ye et al., 1997; Clendenen et al., 2003; Rajić et al., 2023). Although we cannot preclude the possibility of a new underplating system below the trenchward coastal area, the short wavelength (~10 Myr cooling age difference and a doubling of exhumation rate across 10–15 km) of the across-strike changes in the AHe age

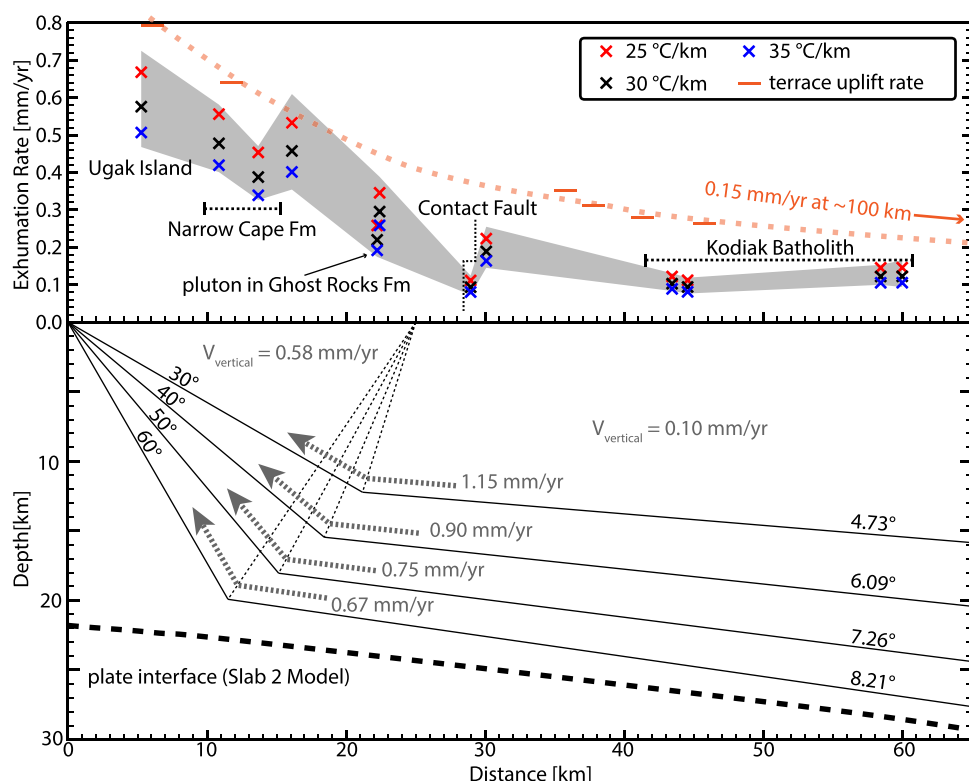


Fig. 7. A trench-normal profile of estimated exhumation rates of apatite (U-Th)/He (AHe) samples (crosses) and uplift rates of marine terraces (upper panel) and estimated possible combinations of overall KSFZ fault geometries and slip rates by assuming various frontal dip angles (lower panel). Three sets of exhumation rate estimations assumed an initial geothermal gradient of 25 °C/km, 30 °C/km and 35 °C/km (red, black and blue symbols, respectively). Gray shadow represents max-min uncertainties calculated from uncertainties of AHe ages. Marine terrace uplift rates were estimated based on the terrace elevation measurements and age assumption by Carver et al. (2008). Fault geometries and average slip rates were estimated based on the long-term exhumation rate pattern revealed by AHe ages. The profile starts at the offshore Ugak Fault (Distance = 186 km on Fig. 8 profile).

and exhumation rate suggests that underplating is unlikely the determining cause of the new exhumation pattern. The Pliocene AHe ages spatially coincide with the documented active faults in the Narrow Cape area and are within about 20 km from the fault traces of the offshore Kodiak Shelf Fault Zone (Fig. 4), suggesting that this exhumation episode is mainly affected by the hanging-wall uplift of the active Kodiak Shelf Fault Zone. Therefore, the initiation of the Kodiak Shelf Fault Zone is likely also 6–7 Ma. This interpretation is consistent with the lithologic study of the latest Miocene-Pliocene Albatross sedimentary sequence on the hanging-wall side of the fault zone, which suggests an upward decrease in clasts from the uplifted shelf break (decrease in chert and total absence of calcareous shale in the upper part) and an increase in clasts from the Kodiak Islands as well as the shallowing of the depositional environment from shallow marine to terrestrial (Clendenen et al., 1992). The initiation of the Kodiak Shelf Fault Zone might have uplifted the basin in its hanging wall and interrupted the transport path of clasts from the shelf break.

Assuming that exhumation is related to throw on the Kodiak Shelf Fault Zone, our new results on spatial variations in exhumation rate can place constraints on the deep geometry of the fault zone. Most of the Kodiak Islands have been experiencing slow exhumation after 15 Ma, and the rapid Pliocene exhumation is limited in the trenchward coastal area approximately southeast of the Contact Fault, close to the main offshore Kodiak Shelf Fault Zone traces (Fig. 7). This pattern suggests that the landward-dipping Kodiak Shelf Fault Zone may become gently dipping beneath the Kodiak Islands (Fig. 8). Assuming the varied exhumation is caused by pure dip-slip along the Kodiak Shelf Fault Zone with a fault bend separating a steep frontal ramp from a deeper gentle flat, we semi-quantitatively estimate the deep geometry. If we assume that the exhumation is balanced by uplift and the uplift rates are the vertical components of fault-slip rates, we can calculate the corresponding fault slip rate and dip of the gentle decollement for a given dip of the frontal thrust ramp. We use the calculated exhumation rates of Ugak Island (0.59 mm/yr for an initial geothermal gradient 30 °C/km) and the Kodiak Batholith (0.1 mm/yr) as uplift rates above the two fault domains. For a frontal dip of 30, 40, 50 and 60°, we estimate the corresponding dip-slip rates are 1.15 mm/yr, 0.90 mm/yr, 0.75 mm/yr and 0.67 mm/yr, respectively, and the corresponding dips of the fault flat beneath the Kodiak Islands are roughly 5, 6, 7 and 8° respectively (Fig. 7). Assuming the bisector of the fault bend projects to the exhumation rate change at the surface, we can construct the general fault geometry. These slip rate estimations do not include lateral strike-slip components, but this simplification does not affect geometry estimations because we assume only dip slip contributes to uplift. We find that even a steep 60-degree Kodiak Shelf Fault Zone frontal thrust cannot directly connect to the subduction interface (Hayes et al., 2018) before it

becomes flat and subparallel to the interface at a depth of about 20 km. The more realistic 30-degree frontal thrust requires the fault flattening at a depth of about 12 km. The flat section can be approximately correlated to an abrupt change in the seismically-determined V_p/V_s ratio within the wedge (Fig. 8, Wang et al., 2024). Therefore, the fault may root into deep structures and may be associated with mechanical property changes within the wedge rather than the subduction interface. The Contact Fault, which likely played a similar role to the KSFZ as an older out-of-sequence thrust fault, may have been offset by younger faults or the active KSFZ at depth. If its shallow part is active, it may branch into the KSFZ flat. A 30-degree geometry of the frontal thrust of the KSFZ also requires a fault slip rate of 1.15 mm/yr, which is about 2% of the present plate convergence rate of 57 mm/yr (DeMets et al., 1990). If so, only a small portion of the plate convergence has been accommodated by the Kodiak Shelf Fault Zone since its presumed initiation at 6–7 Ma. Elliott and Freymueller (2020) estimated GPS-data-derived left-lateral and compressional deformation rates of 2.2 ± 0.3 mm/yr and 3.5 ± 0.4 mm/yr, respectively, approximately across the Kodiak Shelf Fault Zone. The much higher geodetic compressional rate than our estimated long-term dip-slip rate may suggest only a portion of the interseismic geodetic strain translates to permanent deformation as fault slip along the Kodiak Shelf Fault, assuming the compression remained at a higher rate throughout the history of the Kodiak Shelf Fault.

At shallow depths, the displacement may be distributed along multiple fault strands. Ramos et al. (2022) previously recognized the Ugak Fault, the primary offshore strand of the Kodiak Shelf Fault Zone, from bathymetry data and legacy seismic profiles. Using recent bathymetry data and archived seismic images collected in 1975, we mapped more active fault strands in the Ugak Island area (Figs. 3 and S1). They exhibit linear fault and/or fold scarps on the seafloor. On the seismic reflective images, they offset young deposits and occasionally show growth strata. Seismic images also show the Ugak Fault has the most prominent offset (Fig. S1). Previous onshore geomorphologic and paleoseismological studies (e.g., Carver et al., 2008) and our bedrock-structure survey along the coastal cliff in the Narrow Cape area also highlight multiple high-angle faults. The high-angle faults we observed are in the core of a broad 3-km wide anticline formed within the Narrow Cape Formation and its underlying unconformity. We interpret them as shallow faults accommodating passive deformation above a blind thrust fault strand below the broad anticline or as fault strands that mainly accommodate strike-slip displacement and may merge together at depth (Fig. 8).

5.3. Kodiak Shelf Fault Zone development mechanism

Reactivation of inherited structures as a mechanism for upper-plate out-of-sequence thrusting is common in many accretionary complexes,

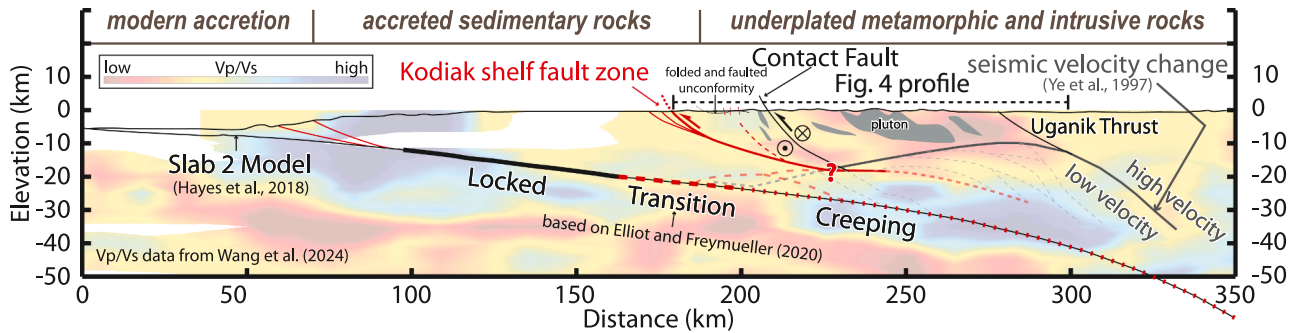


Fig. 8. A cross-section explaining recent exhumation history and a structural model. The subduction interface geometry is based on Slab 2 (Hayes et al., 2018). The thick gray line is the normal-to-section projection of a major seismic velocity change documented by Ye et al. (1997) on the EDGE transect approximately 100 km northeast of the Kodiak Islands. The upper and lower ends of the locked-creeping transition are interpreted based on the subduction interface coupling coefficient in the Kodiak region reported by Elliott and Freymueller (2020). The up-dip limit of the locked segment is schematic. The grey dashed lines represent the hypothesized structural grain based on the available data. The red lines represent known (solid lines) and schematic (dashed lines) active faults. The V_p/V_s data is along a transect across the Kodiak Islands subparallel to our profile (Wang et al. 2024).

such as the Shimanto accretionary complex in Japan (Fisher et al., 2019). The development of the Kodiak Shelf Fault Zone may have exploited the preexisting upper-plate lithologic architecture. The fault system has developed along an approximate boundary in the forearc between lithologies with different mechanical properties (Fig. 8). At shallow levels, the landward side of the fault system is mainly composed of stronger, less permeable and porous underplated and accreted metamorphosed and igneous rocks, such as the Ghost Rocks Formation, the Kodiak Formation, igneous plutons, and the late Triassic to early Jurassic accretionary complex. The trenchward side of the fault system is mainly composed of weaker, more permeable and porous accreted rocks that offscraped from the subduction plate represented by the Sitkalidak Formation and younger units (Moore and Allwardt, 1980; Byrne and Fisher, 1987). The first-order across-fault lithology and mechanical property changes are also exhibited by a low seismically-determined V_p/V_s ratio on the arcward side of the island and an increased V_p/V_s ratio on the trenchward side, where the higher V_p/V_s values are usually interpreted as indicative of elevated fluid content (Wang et al., 2024). The strong contrast in mechanical properties is also suggested by across-strike changes in seismic velocity, gravity and magnetic field data (Song and Simons, 2003; Wells et al., 2003; Ramos et al., 2022; Wang et al., 2024).

At depths beneath the Kodiak Islands, our estimated fault flat geometry of the Kodiak Shelf Fault is located approximately where there is a high gradient in the seismically-determined V_p/V_s ratio at depths of about 15–20 km within the wedge (Fig. 8). Because the duplex structure may have developed through the mainly Eocene-Oligocene underplating process beneath the Kodiak Islands, the change in V_p/V_s ratio may represent the roof of the duplex structure, i.e., the contact between the underplated material and the stronger, less permeable and less porous metamorphosed and igneous rocks exposed at the surface. The low porosity-permeability rocks, suggested by low V_p/V_s values in the upper crustal part of the wedge may have facilitated the trapping of fluids released from the dehydration of the subducting slab within the underplated rocks, which are characterized by high V_p/V_s values. On the EDGE deep seismic reflection image, approximately 100 km northeast of the Kodiak Islands, a deep arch-shaped high-to-low transition of seismic velocity similar to the large V_p/V_s ratio change in the Kodiak Islands area has been identified and interpreted as the top of the low-velocity underplated material (Fig. 8; Moore et al., 1991; Ye et al., 1997). Therefore, although speculative, it is possible that the flat part of the Kodiak Shelf Fault Zone was developed by exploiting the shear zones of the old duplex system, including the roof thrust. The process might have been facilitated by fluid-influenced mechanical property contrast. The linkage between a similar forearc splay fault and a duplex structure along the subduction interface was suggested based on the seismic images in Prince William Sound, about 300 km northeast along-strike (Haeussler et al., 2015).

Previous studies suggest that the interface coupling pattern and seismic behavior along the subduction interface may have been significantly affected by fluid distribution because of its influence on pore-fluid pressure and rheology (e.g. Shillington et al., 2015; Li et al., 2018; Fisher and Hirth, 2024; Wang et al., 2024). Given the coincidence between the inferred Kodiak Shelf Fault geometry and the V_p/V_s pattern (Wang et al., 2024), we envision that the lithology-influenced forearc fluid distribution may have facilitated the long-term continuous deformation along the Kodiak Shelf Fault. Once the splay fault system was established, its damage zone may function as a fluid conduit for releasing the fluid trapped beneath the low porosity-permeability rocks exposed on the Kodiak Islands. Although there is no direct evidence of the process along this offshore fault system, a fluid-rich damage zone has been reported along an ancient out-of-sequence thrust, Uganik Thrust, on the Kodiak Islands (Rowe et al., 2009). The fluid saturation along the fault system can significantly reduce the yield strength and facilitate persistent long-term fault activity.

Because the shallow portion of the KSFZ lies above the approximate

locked-creeping boundary of the megathrust, earthquakes along the KSFZ may be triggered by upper-plate stress changes during megathrust events. If our predicted fault geometry is correct, the KSFZ could also rupture independently in upper-plate earthquakes without major megathrust earthquakes.

6. Conclusions

Most of our ZHe ages record cooling through ZHe closure temperature in the late Eocene-early Oligocene, and are temporally and spatially consistent with the Eocene-early Oligocene broad antiformal exhumation previously documented by zircon and apatite fission track thermochronological ages. However, our AHe ages reveal a new pattern; the ages record cooling through the AHe closure temperature from early Miocene to Pliocene and exhibit an overall decrease trenchward, with Pliocene ages (3–5 Ma) collected from the trenchward coastal area of the Kodiak Islands. Our thermal history modeling suggests that the trenchward coastal area of the Kodiak Islands experienced a change from early-middle Miocene basin subsidence to recent deformation and rapid uplift since 6–7 Ma. In contrast, the rest of the island experienced an early-middle Miocene transition from the prolonged relatively rapid Eocene-Oligocene exhumation to a slow exhumation phase starting approximately in the late Miocene. The early-middle Miocene change in the exhumation pattern might be caused by a change in the dominant deformation mechanism affecting the Kodiak Islands, from broad underplating along the subduction interface to the hanging-wall uplift of the Kodiak Shelf Fault Zone, an active crustal splay fault system above the down-dip edge of the seismogenic zone. The observation that the newly revealed post-Miocene long-term exhumation pattern resembles the estimated uplift patterns based on elevated Pleistocene marine terraces and decadal geodetic data suggests that the splay-fault-related exhumation has persisted from Miocene to Recent. The inherited upper-plate structures and lithologic architecture may affect the fluid distribution (and possibly pore fluid pressure), and therefore effective rock strength in the forearc wedge in a way that facilitates the development of the Kodiak Shelf Fault and its persistent deformation over geological time.

CRediT authorship contribution statement

Suoya Fan: Writing – original draft, Visualization, Methodology, Investigation, Formal analysis, Conceptualization. **Kristin D. Morell:** Writing – original draft, Supervision, Resources, Project administration, Methodology, Investigation, Funding acquisition, Conceptualization. **Donald M. Fisher:** Writing – review & editing, Investigation, Conceptualization. **Hugues Raimbourg:** Writing – review & editing, Investigation, Conceptualization. **Vincent Famin:** Writing – review & editing, Investigation, Conceptualization. **Kristijan Rajic:** Writing – review & editing, Investigation, Conceptualization.

Declaration of competing interest

The authors declare that they have no known competing financial interests or personal relationships that could have appeared to influence the work reported in this paper.

Acknowledgements

This work was primarily funded by NSF grant EAR-2046278 to K. Morell. The authors are grateful to P. Haeussler for his insight in this work. The authors thank Fan Wang for providing the high-resolution profile of V_p/V_s data (Wang et al., 2024) used in Fig. 8. The authors also thank J. Metcalf (CU TRaIL) and A. Kylander-Clark (UC Santa Barbara) for their help with the zircon and apatite (U-Th)/He dating and zircon U-Pb dating analyses, respectively. The authors thank Donna Shillington and Eva Enkelmann for their comments and suggestions that

improved the manuscript.

Supplementary materials

Supplementary material associated with this article can be found, in the online version, at [doi:10.1016/j.epsl.2024.119140](https://doi.org/10.1016/j.epsl.2024.119140).

Data availability

Data is available in Supplemental File.

References

Barker, D.H.N., Henrys, S., Caratori Tontini, F., Barnes, P.M., Bassett, D., Todd, E., Wallace, L., 2018. Geophysical Constraints on the Relationship Between Seamount Subduction, Slow Slip, and Tremor at the North Hikurangi Subduction Zone, New Zealand. *Geophys. Res. Lett.* 45 (23). <https://doi.org/10.1029/2018gl080259>.

Barnes, P.M., Wallace, L.M., Saffer, D.M., Bell, R.E., Underwood, M.B., Fagereng, A., Meneghini, F., Savage, H.M., Rabinowitz, H.S., Morgan, J.K., Kitajima, H., Kutterolf, S., Hashimoto, Y., Engelmann de Oliveira, C.H., Noda, A., Crundwell, M.P., Shepherd, C.L., Woodhouse, A.D., Harris, R.N., Wang, M., Henrys, S., Barker, D.H.N., Petronotis, K.E., Bourlange, S.M., Clemnell, M.B., Cook, A.E., Dugan, B.E., Elger, J., Fulton, P.M., Gamboa, D., Greve, A., Han, S., Hípér, A., Ikari, M.J., Ito, Y., Kim, G.Y., Koge, H., Lee, H., Li, X., Luo, M., Malie, P.R., Moore, G.F., Mountjoy, J.J., McNamara, D.D., Paganoni, M., Scream, E.J., Shankar, U., Shreedharan, S., Solomon, E.A., Wang, X., Wu, H.-Y., Pecher, I.A., LeVay, L.J., 2020. Slow slip source characterized by lithological and geometric heterogeneity. *Sci. Adv.* 6 (13), eaay3314. <https://doi.org/10.1126/sciadv.aay3314>.

Burns, L.E., 1985. The Border Ranges ultramafic and mafic complex, south-central Alaska: cumulate fractionates of island-arc volcanics. *Can. J. Earth. Sci.* 22 (7), 1020–1038. <https://doi.org/10.1139/e85-106>.

Byrne, T., 1984. Early deformation in melange terranes of the ghost rocks formation, Kodiak Islands, Alaska, in Raymond, L. A., ed., *Melanges: their nature, origin, and significance*. *Geol. Soc. Am.* 198, 21–51. <https://doi.org/10.1130/SPE198-p21>.

Byrne, T., 1986. Eocene underplating along the Kodiak Shelf, Alaska: Implications and regional correlations. *Tectonics* 5 (3), 403–421. <https://doi.org/10.1029/TC005i003p00403>.

Byrne, T., Fisher, D., 1987. Episodic growth of the Kodiak convergent margin. *Nature* 325 (6102), 338–341. <https://doi.org/10.1038/325338a0>.

Carden, J.R., Connelly, W., Forbes, R.B., Turner, D.L., 1977. Blueschists of the Kodiak Islands, Alaska: An extension of the Seldovia schist terrane. *Geology* 5 (9), 529–533. [https://doi.org/10.1130/0091-7613\(1977\)5<529:Botkia>2.0.Co;2](https://doi.org/10.1130/0091-7613(1977)5<529:Botkia>2.0.Co;2).

Carver, G., Sauber, J., Lettis, W., Witter, R., Whitney, B., Freymueller, J., 2008. Active faults on northeastern Kodiak Island, Alaska: Active tectonics and seismic potential of Alaska. *Am. Geophys. Union Geophys. Monogr.* 179, 167–184.

Clendenen, W.S., Fisher, D., Byrne, T., Sisson, V.B., Roeske, S.M., Pavlis, T.L., 2003. Cooling and exhumation history of the Kodiak accretionary prism, southwest Alaska, in Sisson, V. B., Roeske, S. M., and Pavlis, T. L., eds., *Geology of a transpressional orogen developed during ridge-trench interaction along the North Pacific margin*, Volume 371: boulder, Colorado. *Geol. Soc. Am. Spec. Pap.* 371, 71–88. <https://doi.org/10.1130/0-8137-2371-x.71>.

Clendenen, W.S., Sliter, W.V., Byrne, T., 1992. Tectonic implications of the Albatross sedimentary sequence, Slatkinak Island, Alaska.

Connelly, W., 1978. Uyak Complex, Kodiak Islands, Alaska: A Cretaceous subduction complex. *GSA Bull.* 89 (5), 755–769. [https://doi.org/10.1130/0016-7606\(1978\)89<755:UCKIAA>2.0.CO;2](https://doi.org/10.1130/0016-7606(1978)89<755:UCKIAA>2.0.CO;2).

Cook, B.J., Henstock, T.J., McNeill, L.C., Bull, J.M., 2014. Controls on spatial and temporal evolution of prism faulting and relationships to plate boundary slip offshore north-central Sumatra. *J. Geophys. Res.: Solid Earth* 119 (7), 5594–5612. <https://doi.org/10.1002/2013jb010834>.

Cummins, P.R., Kaneda, Y., 2000. Possible splay fault slip during the 1946 Nankai earthquake. *Geophys. Res. Lett.* 27 (17), 2725–2728. <https://doi.org/10.1029/1999GL011139>.

Davies, J., Sykes, L., House, L., Jacob, K., 1981. Shumagin seismic gap, Alaska Peninsula – history of great earthquakes, tectonic setting, and evidence for high seismic potential. *J. Geophys. Res.* 86 (Nb5), 3821–3855. <https://doi.org/10.1029/JB086IB05p03821>.

DeMets, C., Gordon, R.G., Argus, D.F., Stein, S., 1990. Current plate motions. *Geophys. J. Int.* 101 (2), 425–478. <https://doi.org/10.1111/j.1365-246X.1990.tb06579.x>.

DePaolis, J.M., Dura, T., Witter, R.C., Haeussler, P.J., Bender, A., Curran, J.H., Corbett, D.R., 2024. Repeated coseismic uplift of coastal lagoons above the Patton Bay splay fault system, Montague Island, Alaska, USA. *J. Geophys. Res.: Solid Earth* 129 (5). <https://doi.org/10.1029/2023jb028552>.

Dielforder, A., Hetzel, R., Oncken, O., 2020. Megathrust shear force controls mountain height at convergent plate margins. *Nature* 582 (7811), 225–229. <https://doi.org/10.1038/s41586-020-2340-7>.

Elliott, J., Freymueller, J.T., 2020. A block model of present-day kinematics of Alaska and Western Canada. *J. Geophys. Res.: Solid Earth* 125 (7), e2019JB018378. <https://doi.org/10.1029/2019JB018378>.

Farris, D.W., 2010. Tectonic and petrologic evolution of the Kodiak batholith and the trenchward belt, Kodiak Island, AK: Contact fault juxtaposition? *J. Geophys. Res.* 115 (B7). <https://doi.org/10.1029/2009jb006434>.

Farris, D.W., Haeussler, P., Friedman, R., Paterson, S.R., Saltus, R.W., Ayuso, R., 2006. Emplacement of the Kodiak batholith and slab-window migration. *Geol. Soc. Am. Bull.* 118 (11–12), 1360–1376. <https://doi.org/10.1130/b25718.1>.

Fisher, D., Byrne, T., 1987. Structural evolution of underthrusted sediments, Kodiak Islands, Alaska. *Tectonics* 6 (6), 775–793. <https://doi.org/10.1029/TC006i006p00775>.

Fisher, D.M., Byrne, T., 1992. Strain variations in an ancient accretionary complex: implications for forearc evolution. *Tectonics* 11 (2), 330–347. <https://doi.org/10.1029/91tc01490>.

Fisher, D.M., Hirth, G., 2024. A pressure solution flow law for the seismogenic zone: application to Cascadia. *Sci. Adv.* 10 (4), eadi7279. <https://doi.org/10.1126/sciadv.adi7279>.

Fisher, D.M., Tonai, S., Hashimoto, Y., Tomioka, N., Oakley, D., 2019. K-Ar Dating of Fossil Seismogenic Thrusts in the Shimanto Accretionary Complex, Southwest Japan. *Tectonics* 38 (11), 3866–3880. <https://doi.org/10.1029/2019TC005571>.

Fisher, M.A., Holmes, M.L., 1980. Large-scale structure of deep strata beneath Kodiak shelf, Alaska. *GSA Bull.* 91 (4), 218–224. [https://doi.org/10.1130/0016-7606\(1980\)91<218:Lsodsb>2.0.Co;2](https://doi.org/10.1130/0016-7606(1980)91<218:Lsodsb>2.0.Co;2).

Flowers, R.M., Ketcham, R.A., Shuster, D.L., Farley, K.A., 2009. Apatite (U-Th)/He thermochronometry using a radiation damage accumulation and annealing model. *Geochim. et Cosmochimica Acta* 73 (8), 2347–2365. <https://doi.org/10.1016/j.gca.2009.01.015>.

Haeussler, P.J., Armstrong, P.A., Liberty, L.M., Ferguson, K.M., Finn, S.P., Arkle, J.C., Pratt, T.L., 2015. Focused exhumation along megathrust splay faults in Prince William Sound, Alaska. *Quatern. Sci. Rev.* 113, 8–22. <https://doi.org/10.1016/j.quascirev.2014.10.013>.

Haeussler, P.J., Bradley, D.C., Wells, R.E., Miller, M.L., 2003. Life and death of the Resurrection plate: evidence for its existence and subduction in the northeastern Pacific in Paleocene–Eocene time. *GSA Bull.* 115 (7), 867–880. [https://doi.org/10.1130/0016-7606\(2003\)115<0867:Ladot>2.0.Co;2](https://doi.org/10.1130/0016-7606(2003)115<0867:Ladot>2.0.Co;2).

Hayes, G.P., Moore, G.L., Portner, D.E., Hearne, M., Flamme, H., Furtney, M., Smoczyk, G.M., 2018. Slab2, a comprehensive subduction zone geometry model. *Science* 362 (6410), 58–61. <https://doi.org/10.1126/science.aat4723>.

Jolivet, R., Simons, M., Duputel, Z., Olive, J.-A., Bhat, H.S., Bletry, Q., 2020. Interseismic Loading of Subduction Megathrust Drives Long-Term Uplift in Northern Chile. *Geophys. Res. Lett.* 47 (8), e2019GL085377. <https://doi.org/10.1029/2019GL085377>.

Ketcham, R.A., 2005. Forward and inverse modeling of low-temperature thermochronometry data. *Rev. Mineral. Geochem.* 58 (1), 275–314. <https://doi.org/10.2138/rmg.2005.58.11>.

Kimura, G., Kitamura, Y., Hashimoto, Y., Yamaguchi, A., Shibata, T., Ujiie, K., Okamoto, S.y., 2007. Transition of accretionary wedge structures around the up-dip limit of the seismogenic subduction zone. *Earth Planet. Sci. Lett.* 255 (3), 471–484. <https://doi.org/10.1016/j.epsl.2007.01.005>.

Li, J., Shillington, D.J., Saffer, D.M., Bécel, A., Nedimović, M.R., Kuehn, H., Webb, S.C., Keranen, K.M., Abers, G.A., 2018. Connections between subducted sediment, pore-fluid pressure, and earthquake behavior along the Alaska megathrust. *Geology* 46 (4), 299–302. <https://doi.org/10.1130/g39557.1>.

Liberty, L.M., Brothers, D.S., Haeussler, P.J., 2019. Tsunamigenic splay faults imply a long-term asperity in Southern Prince William Sound, Alaska. *Geophys. Res. Lett.* 46 (7), 3764–3772. <https://doi.org/10.1029/2018gl081528>.

Liberty, L.M., Finn, S.P., Haeussler, P.J., Pratt, T.L., Peterson, A., 2013. Megathrust splay faults at the focus of the Prince William Sound asperity, Alaska. *J. Geophys. Res.: Solid Earth* 118 (10), 5428–5441. <https://doi.org/10.1002/jgrb.50372>.

Liu, C., Lay, T., Xiong, X., 2022. The 29 July 2021 M-W 8.2 Chignik, Alaska Peninsula Earthquake rupture inferred from seismic and geodetic observations: re-rupture of the Western 2/3 of the 1938 Rupture Zone. *Geophys. Res. Lett.* 49 (4). <https://doi.org/10.1029/2021gl096004>.

Marinovich Jr, L., Moriya, S., 1992. Early middle Miocene mollusks and benthic foraminifers from Kodiak Island, Alaska.

Michel-Wolf, L., Ehlers, T.A., Bendick, R., 2022. Transitions in subduction zone properties align with long-term topographic growth (Cascadia, USA). *Earth Planet. Sci. Lett.* 580. <https://doi.org/10.1016/j.epsl.2021.117363>.

Moore, G.F., Bangs, N.L., Taira, A., Kuramoto, S., Pangborn, E., Tobin, H.J., 2007. Three-dimensional splay fault geometry and implications for tsunami generation. *Science* 318 (5853), 1128–1131. <https://doi.org/10.1126/science.1147195>.

Moore, J.C., 1978. Orientation of underthrusting during latest Cretaceous and earliest Tertiary time, Kodiak Islands, Alaska. *Geology* 6 (4), 209–213. [https://doi.org/10.1130/0091-7613\(1978\)6<209:Ooudlc>2.0.Co;2](https://doi.org/10.1130/0091-7613(1978)6<209:Ooudlc>2.0.Co;2).

Moore, J.C., Allwardt, A., 1980. Progressive deformation of a Tertiary Trench Slope, Kodiak Islands, Alaska. *J. Geophys. Res.: Solid Earth* 85 (B9), 4741–4756. <https://doi.org/10.1029/JB085IB09p04741>.

Moore, J.C., Byrne, T., Plumley, P.W., Reid, M., Gibbons, H., Coe, R.S., 1983. Paleogene evolution of the Kodiak Islands, Alaska: Consequences of ridge-trench interaction in a more southerly latitude. *Tectonics* 2 (3), 265–293. <https://doi.org/10.1029/TC002i003p00265>.

Moore, J.C., Diebold, J., Fisher, M.A., Sample, J., Brocher, T., Talwani, M., Ewing, J., Huene, R.v., Rowe, C., Stone, D., Stevens, C., Sawyer, D., 1991. EDGE deep seismic reflection transect of the eastern Aleutian arc-trench layered lower crust reveals underplating and continental growth. *Geology* 19 (5), 420–424. [https://doi.org/10.1130/0091-7613\(1991\)019<0420:EDSRTO>2.3.CO;2](https://doi.org/10.1130/0091-7613(1991)019<0420:EDSRTO>2.3.CO;2).

Nilsen, T.H., and Moore, G.W., 1979. Reconnaissance study of Upper Cretaceous to Miocene stratigraphic units and sedimentary facies, Kodiak and adjacent islands, Alaska, with a section on sedimentary petrography.

Oryan, B., Olive, J.-A., Jolivet, R., Malatesta, L.C., Gailleton, B., Bruhat, L., 2024. Megathrust locking encoded in subduction landscapes. *Sci. Adv.* 10 (17), ead14286. <https://doi.org/10.1126/sciadv.adl4286>.

Park, J.-O., Tsuru, T., Kodaira, S., Cummings, P.R., Kaneda, Y., 2002. Splay Fault Branching Along the Nankai Subduction Zone. *Science* 297 (5584), 1157–1160. <https://doi.org/10.1126/science.1074111>.

Plafker, G., 1965. Tectonic deformation associated with the 1964 Alaska earthquake. *Science* 148 (3678), 1675–1687. <https://doi.org/10.1126/science.148.3678.1675>.

Qin, Y., Chen, J., Singh, S.C., Hananto, N., Carton, H., Tappognier, P., 2024. Assessing the Risk of Potential Tsunamigenic Earthquakes in the Mentawai Region by Seismic Imaging, Central Sumatra. *Geochem. Geophys. Geosyst.* 25 (5). <https://doi.org/10.1029/2023gc011149>.

Rajić, K., Raimbourg, H., Famin, V., Moris-Muttoni, B., Fisher, D.M., Morell, K.D., Canizarés, A., 2023. Exhuming an accretionary prism: a case study of the Kodiak accretionary complex, Alaska, USA. *Tectonics* 42 (10). <https://doi.org/10.1029/2023tc007754>.

Ramos, M.D., Liberty, L.M., Haeussler, P.J., Humphreys, R., 2022. Upper-plate structure and tsunamigenic faults near the Kodiak Islands, Alaska, USA. *Geosphere* 18 (5), 1474–1491. <https://doi.org/10.1130/ges02486.1>.

Reiners, P.W., 2005. Zircon (U-Th)/He thermochronometry. *Rev. Mineral. Geochem.* 58 (1), 151–179. <https://doi.org/10.2138/rmg.2005.58.6>.

Reiners, P.W., Spell, T.L., Niculescu, S., Zanetti, K.A., 2004. Zircon (U-Th)/He thermochronometry: He diffusion and comparisons with 40Ar/39Ar dating. *Geochimica et Cosmochimica Acta* 68 (8), 1857–1887. <https://doi.org/10.1016/j.gca.2003.10.021>.

Roeske, S.M., Mattinson, J.M., Armstrong, R.L., 1989. Isotopic ages of glaucophane schists on the Kodiak Islands, southern Alaska, and their implications for the Mesozoic tectonic history of the Border Ranges fault system. *Geol. Soc. Am. Bull.* 101 (8), 1021–1037. [https://doi.org/10.1130/0016-7606\(1989\)101<1021:IAOGSO>2.3.CO;2](https://doi.org/10.1130/0016-7606(1989)101<1021:IAOGSO>2.3.CO;2).

Rowe, C.D., Meneghini, F., Moore, J.C., 2009. Fluid-rich damage zone of an ancient out-of-sequence thrust, Kodiak Islands, Alaska. *Tectonics* 28 (1). <https://doi.org/10.1029/2007TC002126>.

Saillard, M., Audin, L., Rousset, B., Avouac, J.-P., Chlieh, M., Hall, S.R., Husson, L., Farber, D.L., 2017. From the seismic cycle to long-term deformation: linking seismic coupling and Quaternary coastal geomorphology along the Andean megathrust. *Tectonics* 36 (2), 241–256. <https://doi.org/10.1002/2016TC004156>.

Sample, J.C., Fisher, D.M., 1986. Duplex accretion and underthrusting in an ancient accretionary complex, Kodiak Islands, Alaska. *Geology* 14 (2), 160–163. [https://doi.org/10.1130/0091-7613\(1986\)14<160:Daaua>2.0.Co;2](https://doi.org/10.1130/0091-7613(1986)14<160:Daaua>2.0.Co;2).

Sample, J.C., Moore, J.C., 1987. Structural style and kinematics of an underthrust slate belt, Kodiak and adjacent islands, Alaska. *GSA Bull.* 99 (1), 7–20. [https://doi.org/10.1130/0016-7606\(1987\)99<7:Ssakoa>2.0.Co;2](https://doi.org/10.1130/0016-7606(1987)99<7:Ssakoa>2.0.Co;2).

Sample, J.C., Reid, M.R., 2003. Large-scale, latest Cretaceous uplift along the Northeast Pacific Rim: evidence from sediment volume, sandstone petrography, and Nd isotope signatures of the Kodiak Formation, Kodiak Islands, Alaska, in Sisson, V. B., Roeske, S. M., and Pavlis, T. L., eds. *Geology of a transpressional orogen developed during ridge-trench interaction along the North Pacific margin*, Volume 371, Geological Society of America 0. <https://doi.org/10.1130/0-8137-2371-x.51>.

Sauber, J., Carver, G., Cohen, S., King, R., 2006. Crustal deformation and the seismic cycle across the Kodiak Islands, Alaska. *J. Geophys. Res.: Solid Earth* 111 (B2). <https://doi.org/10.1029/2005JB003626>.

Shillington, D.J., Bécel, A., Nedimović, M.R., Kuehn, H., Webb, S.C., Abers, G.A., Keranen, K.M., Li, J., Delescluse, M., Mattei-Salicrup, G.A., 2015. Link between plate fabric, hydration and subduction zone seismicity in Alaska. *Nat. Geosci.* 8 (12), 961–964. <https://doi.org/10.1038/ngeo2586>.

Sibuet, J., Rangin, C., Lepichon, X., Singh, S., Cattaneo, A., Graindorge, D., Klingelhoefer, F., Lin, J., Malod, J., Maury, T., 2007. 26th December 2004 great Sumatra–Andaman earthquake: Co-seismic and post-seismic motions in northern Sumatra. *Earth Planet. Sci. Lett.* 263 (1–2), 88–103. <https://doi.org/10.1016/j.epsl.2007.09.005>.

Song, T.-R.A., Simons, M., 2003. Large trench-parallel gravity variations predict seismogenic behavior in subduction zones. *Science* 301 (5633), 630–633. <https://doi.org/10.1126/science.1085557>.

Strasser, M., Moore, G.F., Kimura, G., Kitamura, Y., Kopf, A.J., Lallemand, S., Park, J.-O., Screamton, E.J., Su, X., Underwood, M.B., Zhao, X., 2009. Origin and evolution of a splay fault in the Nankai accretionary wedge. *Nat. Geosci.* 2 (9), 648–652. <https://doi.org/10.1038/ngeo609>.

Suito, H., Freymueller, J.T., 2009. A viscoelastic and afterslip postseismic deformation model for the 1964 Alaska earthquake. *J. Geophys. Res.: Solid Earth* 114 (B11). <https://doi.org/10.1029/2008jb005954>.

Suleiman, E., Freymueller, J.T., 2020. Near-field modeling of the 1964 Alaska Tsunami: the role of splay faults and horizontal displacements. *J. Geophys. Res.: Solid Earth* 125 (7). <https://doi.org/10.1029/2020jb019620>.

van der Beek, P., Schilgen, T.F., 2023. Short communication: age2exhume – a MATLAB/Python script to calculate steady-state vertical exhumation rates from thermochronometric ages and application to the Himalaya. *Geochronology* 5 (1), 35–49. <https://doi.org/10.5194/gchron-5-35-2023>.

van Zelst, I., Rannabauer, L., Gabriel, A.A., van Dinther, Y., 2022. Earthquake rupture on multiple splay faults and its effect on tsunamis. *J. Geophys. Res.: Solid Earth* 127 (8). <https://doi.org/10.1029/2022jb024300>.

von Huene, R., Miller, J.J., Krabbenhoft, A., 2021. The Alaska convergent margin backstop splay fault zone, a potential large tsunami generator between the frontal prism and continental framework: geochemistry, geophysics. *Geosystems* 22 (1), e2019GC008901. <https://doi.org/10.1029/2019GC008901>.

Wang, F., Wei, S.S., Drooff, C., Elliott, J.L., Freymueller, J.T., Ruppert, N.A., Zhang, H., 2024. Fluids control along-strike variations in the Alaska megathrust slip. *Earth Planet. Sci. Lett.* 633. <https://doi.org/10.1016/j.epsl.2024.118655>.

Wang, K., Hu, Y., 2006. Accretionary prisms in subduction earthquake cycles: the theory of dynamic Coulomb wedge. *J. Geophys. Res.: Solid Earth* 111 (B6). <https://doi.org/10.1029/2005jb004094>.

Wang, X., Morgan, J., 2022. Effects of coseismic megasplay fault activity on earthquake hazards: insights from discrete element simulations. *J. Struct. Geol.* 155. <https://doi.org/10.1016/j.jsg.2022.104533>.

Wells, R.E., Blakely, R.J., Sugiyama, Y., Scholl, D.W., Dinterman, P.A., 2003. Basin-centered asperities in great subduction zone earthquakes: a link between slip, subsidence, and subduction erosion? *J. Geophys. Res.: Solid Earth* 108 (B10). <https://doi.org/10.1029/2002jb002072>.

Wendt, J., Oglesby, D.D., Geist, E.L., 2009. Tsunamis and splay fault dynamics. *Geophys. Res. Lett.* 36 (15). <https://doi.org/10.1029/2009 gl038295>.

Wilson, F.H., 2013. Reconnaissance geologic map of Kodiak Island and adjacent islands, Alaska. US Geol. Surv., scale 1, 500,000.

Ye, S., Flueh, E.R., Klaeschen, D., von Huene, R., 1997. Crustal structure along the EDGE transect beneath the Kodiak shelf off Alaska derived from OBH seismic refraction data. *Geophys. J. Int.* 130 (2), 283–302. <https://doi.org/10.1111/j.1365-246X.1997.tb05648.x>.